Nanoscale Horizons

COMMUNICATION

Check for updates

Gene silencing regulated by aggregates of Corn aptamer at 3′ UTR of mRNA

Zhuoer Jin,† Yuhan Yang,† Chunfa Chen, Zhe Zhang, Qiao Ren, Zhihong Cui, Cheng Zhi Huang and Hua Zuo *

Gene therapy, as a cutting-edge approach for disease intervention, relies heavily on advancements in gene silencing techniques. For instance, CRISPR-Cas9 has emerged as a leading gene-editing tool due to its ability to introduce precise cuts at specific genomic loci, enabling targeted gene insertion, deletion, or modification. In this study, we developed a simple and effective gene silencing strategy by introducing a nucleic acid self-assembly module into the 3′ untranslated region (UTR) of mRNA. This module demonstrated significant gene silencing efficacy in eukaryotic cells through the formation of RNA aggregates. To systematically investigate its regulatory mechanism on translation efficiency through the formation of higher-order RNA structures, we quantitatively analyzed both mRNA and protein expression levels. Furthermore, our modular 3′ UTR sequences can be integrated with classical 5′ UTR elements (*e.g.*, TOP sequences) to construct a multidimensional post-transcriptional regulatory network. This technology expands the diversity of existing UTR element libraries and offers a reservoir of programmable regulatory elements for applications in synthetic biology. It enables the construction of orthogonal combinations of multidimensional elements, tailored to specific gene expression regulation needs.

New concepts

This study introduces a novel gene silencing strategy utilizing the RNA aptamer Corn, a 28-nucleotide (nt), single-stranded RNA that spontaneously homodimerizes and aggregates into condensate-forming RNA nanostructures, by incorporating it into the 3′ untranslated region (3′ UTR) of eukaryotic mRNA. Incorporation of Corn aptamer into the 3′ UTR induces mRNA aggregation, thereby impairing translation without affecting mRNA stability. This approach is distinct from existing gene silencing methods like RNA interference (RNAi) by utilizing self-assembled RNA nanostructures to obstruct protein translation, instead of directly degrading the mRNA or disrupting gene expression at the transcriptional level. The simplicity of this method, along with its low cytotoxicity and effective gene silencing capability, presents a promising alternative for therapeutic applications in gene therapy. The concept of RNA-induced mRNA aggregation as a gene silencing mechanism offers new insights into how RNA structures can be engineered to regulate gene expression, advancing applications in synthetic biology and biomedicine.

Gene silencing is a fundamental mechanism that controls gene expression by inhibiting transcription or translation of target genes. It plays essential roles in cellular homeostasis,[1–3] genome stability,[4,5] antiviral defense,[6–8] and therapeutic regulation.[9–11] Conventional gene silencing strategies, such as RNA interference (RNAi), antisense oligonucleotides, and CRISPR-Cas-based genome editing, have advanced both basic research and clinical applications. However, these approaches still face key limitations, including off-target effects, incomplete silencing efficiency, and difficulty in achieving multiplexed or reversible regulation. Therefore, developing precise, programmable, and biocompatible post-transcriptional regulation tools remains an important goal for gene therapy and synthetic biology.

In recent years, nucleic acid nanostructures have emerged as versatile platforms for constructing programmable regulatory systems.[12–20] DNA and RNA molecules can self-assemble into defined architectures through predictable base pairing, enabling the creation of nanoscale frameworks for gene delivery,[21–24] molecular sensing,[25–29] biocomputing devices,[30–32] and smart material development.[31,33,34]

With the continued advancement of RNA nanostructure research, their potential in gene silencing has garnered growing interest. Currently, RNA nanostructures primarily achieve targeted gene silencing through the delivery of siRNA, modulation of miRNA levels, ribozyme-mediated cleavage of viral RNAs, and enhancements within CRISPR-Cas9 technology. Guo *et al.* reported the first multivalent RNA nanoparticle for gene silencing, pRNA. Subsequent studies engineered this into an X-shaped RNA nanoparticle, with its four arms complementary-paired to siRNA for targeted gene silencing.[35,36] Jaeger *et al.* utilized inverse kissing loop complexes to form RNA nanorings.

Key Laboratory of Luminescence Analysis and Molecular Sensing (Southwest University), Ministry of Education, College of Pharmaceutical Sciences, Southwest University, Chongqing 400715, China. E-mail: zuohua@swu.edu.cn
† These authors contributed equally to this work.

These siRNA-loaded nanorings were further assembled into nanoparticles, creating multifunctional RNA vectors for targeted gene silencing.[37–39] Lee *et al.* demonstrated that rolling circle amplification generates long RNA strands that self-assemble into sponge-like spherical architectures. Linking multiple siRNAs onto these structures enabled highly efficient gene silencing *in vivo*.[40,41] Roh *et al.* also constructed siRNA nanoparticles *via* rolling circle amplification, which exhibited favorable biostability and tumor-targeting capabilities.[42] Yang *et al.* designed a novel bivalent aptamer-terminus-free siRNA junction nanostructure. This formed *via* the self-assembly and nick ligation of three RNA strands, demonstrating superior gene silencing efficacy.[43] Shapiro *et al.* assembled RNA nanorings functionalized with six shRNAs targeting distinct regions of HIV-1, achieving suppression of HIV replication in cells.[39] Shu *et al.* reported an anti-miR-21 therapeutic agent designed using a pRNA-3WJ motif-based nanostructure, applying in an orthotopic mouse tumor model resulted in tumor regression.[44] Guo group conjugated ribozymes to pRNA or the 3WJ motif and applied them against HBV, enabling cleavage of the HBV genomic RNA and subsequent inhibition of viral replication.[45,46] These show the application of RNA nanostructures for gene silencing holds considerable promise.

In this study, we introduced a tandem repeat of the RNA aptamer, Corn,[47] a 28-nucleotide (nt), single-stranded RNA aptamer containing guanine-rich regions that fold into G-quadruplex structures, spontaneously homodimerize, and aggregate into condensate-forming RNA nanostructures, into the 3′ untranslated region (3′ UTR) of eukaryotic mRNA. These RNA motifs effectively induced gene silencing. Our results revealed that the engineered 3′ UTRs significantly affected both mRNA stability and protein translation efficiency, with their primary regulatory effect exerted at the level of translation. Furthermore, integrating the engineered 3′ UTRs into diverse eukaryotic expression vectors demonstrated the generality of its capability to downregulate recombinant protein expression.

Materials and methods

Ampicillin sodium solution (100 mg mL^{-1}), yeast extract, tryptone, sodium chloride, agar, real-time quantitative PCR 8-tube strips and caps (100 µL), diethylpyrocarbonate (DEPC)-treated water, skimmed milk powder, color pre-stained protein marker (15–130 kDa), Coomassie Brilliant Blue G-250, *N*,*N*'-methylenebisacrylamide, and acrylamide were purchased from Sangon Biotech (Shanghai) Co., Ltd., China. Tris base, glycine, 1.0 M Tris-HCl (pH 6.8), 1.5 M Tris-HCl (pH 8.8), and bicinchoninic acid (BCA) protein quantification kit were obtained from Dingguo Changsheng Biotechnology Co., Ltd., Beijing, China. Acetic acid, isopropanol, and methanol were sourced from Titan Technology Co., Ltd., Shanghai, China. Ammonium persulfate (APS) was purchased from Macklin Biochemical Technology Co., Ltd., Shanghai, China.

Construction of recombinant plasmids

Target gene fragments were amplified by PCR using PrimeSTAR Max DNA Polymerase (Takara). Following separation *via* agarose gel electrophoresis, the target fragments were purified and subsequently ligated into linearized vectors using the Hieff Clone® Universal One Step Cloning Kit (Yeasen Biotechnology, China). The recombinant plasmids were then transformed into *Escherichia coli* Trelief 5α competent cells and cultured at 37 °C overnight. Single colonies were screened for target gene insertion by PCR using 2× GoTaq Green Master Mix (Promega). Colonies yielding positive PCR results were sent to Sangon Biotech (Shanghai) Co., Ltd. for DNA sequencing.

In vitro transcription of RNA

RNA was transcribed *in vitro* from DNA templates using the T7 High Yield RNA Transcription Kit (Novoprotein Scientific). Subsequently, 30 µL of nuclease-free water and 30 µL of 8 M lithium chloride were added to 20 µL of transcription products, followed by thorough mixing. The mixture was incubated at −20 °C for 1 h. After centrifugation, the supernatant was discarded, and the RNA pellet was washed three times with ice-cold 70% ethanol prepared in nuclease-free water. Residual ethanol was removed by SpeedVac drying, and purified RNA was resuspended in nuclease-free water for concentration measurement.

Measurement of melting temperature of RNA

Purified RNA (20 µg) was dissolved in 720 µL of DEPC-treated water and transferred to a 1.5 mL microcentrifuge tube. Subsequently, 80 µL of 10× buffer A (100 mM KCl, 50 mM Tris, 10 mM MgCl$_2$) was added, followed by thorough mixing *via* vortexing. The tube was briefly centrifuged for 1 min to collect droplets from the walls. The sample was then incubated at 37 °C for 30 min in a metal heating block. Following incubation, the solution was transferred to a 1 mL double-path quartz cuvette. UV-Vis absorption spectra were recorded using a UV spectrophotometer in "Thermal" mode under the following parameters: temperature range: 20–95 °C, ramp rate: 1 °C min^{-1}, bandwidth: 2 nm, response time: 4 s, the melting curve of the circular aptamer was monitored at 260 nm.

Analysis of RNA by electrophoresis

For each RNA sample, 2 µg RNA was dissolved in 1 µL 10 × buffer A (100 mM KCl, 50 mM Tris, 10 mM MgCl$_2$) and 2 µL 5× RNA loading buffer. The mixture was adjusted to a final volume of 10 µL by adding DEPC-treated water, thoroughly mixed by vortexing, and briefly centrifuged for 1 min to collect any residual droplets. Samples were then incubated at 37 °C for 30 min. Following incubation, RNA samples were loaded onto a 2% agarose gel to analyze electrophoretic mobility.

Fluorescence analysis of cells by flow cytometry

After post-plasmid transfection for 72 h, the cell culture plate was removed. Complete medium was discarded, and cells were washed three times with PBS buffer. After 1 min of trypsin digestion, digestion was terminated by adding complete medium. Cells were collected into a 2 mL centrifuge tube and centrifuged at 1000 rpm for 5 min. The supernatant was discarded, and the pellet was washed twice with PBS.

Cells were resuspended in 600 μL PBS buffer, filtered through a 200-mesh cell strainer, and immediately subjected to flow cytometry to detect GFP fluorescence intensity. Mean GFP fluorescence intensity of 10 000 cells per sample was measured using the FITC-A channel (excitation laser: 488 nm; emission filter: 530 ± 15 nm) with three biological replicates per group.

Fluorescence analysis of cells by laser confocal microscopy

After post-transfection for 48 h, the cell culture plate was removed. Culture medium was discarded, and cells were washed three times with PBS buffer. Subsequently, 100 μL of 4% paraformaldehyde solution was added to each well to fix cells for 20 min at room temperature. The fixative was discarded, and cells were washed three times with PBS buffer. 3,5-Difluoro-4-hydroxybenzylidene-imidazolinone-2-oxyme (DFHO)solution was then added to each well at a final concentration of 10 μM, followed by incubation at 37 °C for 30 min. After discarding the DFHO solution, cells were washed three times with PBS. DAPI nuclear stain was added and incubated for 10 min at room temperature. The dye was discarded, and cells were washed three times with PBS. Cell climbing sheets were mounted upside-down on glass slides using antifade mounting medium. Cellular fluorescence was observed using laser confocal microscopy.

Evaluation of cellular cytotoxicity

Cells in the logarithmic growth phase with optimal viability were trypsinized and seeded into a 96-well cell culture plate, followed by overnight incubation. When cell density reached 70–80%, transfection was performed with 100 ng plasmid per well. After post-transfection for 24 h, CCK-8 reagent was added and incubated for 1 h. Absorbance at 450 nm was measured for each well, and cell viability was calculated using the following formula:

$$\text{Cell viability (\%)}$$
$$= \frac{\text{Absorbance}_{\text{(treated well)}} - \text{Absorbance}_{\text{(blank well)}}}{\text{Absorbance}_{\text{(untreated cell well)}} - \text{Absorbance}_{\text{(blank well)}}} \times 100\%.$$

Optical density and fluorescence analysis of yeast cells

Single colonies were picked and inoculated into 2 mL SD liquid medium, cultured overnight at 30 °C. Subsequently, 5 μL bacterial culture was diluted to 200 μL with the same SD medium. The mixture was transferred to a 96-well plate, covered with a plate lid, and used for optical density and fluorescence intensity measurements. Using a Synergy H1 Hybrid Reader (BioTek) at 30 °C, OD_{600} (optical density at 600 nm) and fluorescence intensity (excitation: 485 nm; emission: 530 nm) were measured every 2 h for 12 h under continuous shaking. All experiments used at least three randomly selected colonies as biological replicates.

Results and discussion

Eukaryotic mRNA comprises five primary components: the 5′ cap structure, the 5′ UTR upstream of the initiation codon (AUG), the coding sequence (CDS), the 3′ UTR downstream of the termination codon, and the 3′ polyadenylated tail (poly(A) tail). While the 5′ UTR and 3′ UTR do not directly encode proteins, they critically regulate mRNA translation and protein expression.[48] UTRs govern mRNA subcellular localization, translation efficiency, and mRNA stability.[49] Both 5′ and 3′ UTRs modulate protein expression levels: the 5′ UTR primarily regulates translation initiation,[50] whereas the 3′ UTR predominantly influences mRNA stability and half-life.[51]

Impact of Corn on RNA aggregation

During dimerization, neither Corn monomer forms base pairs or helical structures with its counterpart. Based on this, we hypothesized that the Corn RNA aptamer could drive the multimerization of transcribed long mRNAs.

To test this, we engineered the Corn RNA aptamer into the 3′ UTR of mRNA to promote its assembly into multimeric RNA complexes. Specifically, we designed sequences containing 1, 3, 5, or 7 tandem repeats of the aptamer and inserted them into the 3′ UTR of green fluorescent protein (GFP) mRNA to investigate how dimerization-capable Corn structures influence mRNA aggregation (Fig. 1a and Table S1). We first amplified the target gene fragment and linearized the plasmid vector by PCR, then constructed recombinant plasmids for heterologous GFP expression in HEK 293T cells using *in vitro* seamless cloning (Fig. S1). The plasmid architectures are illustrated in Fig. 1b. Based on the number of Corn repeats inserted into the 3′ UTR, the recombinant plasmids were designated as GFP-1 × Corn, GFP-3 × Corn, GFP-5 × Corn, and GFP-7 × Corn. A plasmid containing the wild-type 3′ UTR without Corn insertion was used as a control; after insertion of the GFP gene into its multiple cloning site (MCS), this construct was designated GFP-WT.

Using the recombinant plasmids GFP-1 × Corn, GFP-3 × Corn, GFP-5 × Corn, GFP-7 × Corn, and GFP-WT as templates, we performed PCR to specifically amplify the GFP and 3′ UTR regions, yielding five target DNA fragments (Fig. S2), these fragments were transcribed *in vitro* into corresponding RNA segments, designated 1 × Corn, 3 × Corn, 5 × Corn, 7 × Corn, and WT. Denaturing agarose gel electrophoresis confirmed the expected RNA sizes, minimal degradation, and high purity, thereby supporting their use in subsequent experiments (Fig. S3). Native agarose gel electrophoresis (1%) under intracellular-mimicking buffer conditions revealed that, the 3 × Corn, 5 × Corn, and 7 × Corn samples exhibited slower-migrating bands compared with WT and 1 × Corn, indicating the formation of higher-order RNA structures with more copies of Corn (Fig. 2a). As the number of Corn repeats increased, slower-migrating bands became more prominent, indicating that multimerization of Corn structures hindered RNA electrophoretic mobility. This demonstrated that the engineered Corn RNA aptamer directed the formation of RNA aggregates. We hypothesized that, in a cellular environment, these Corn-induced aggregates could obstruct the nuclear export of GFP mRNA through nuclear pores, thereby mediating gene silencing.

Subsequently, we measured the melting temperature (T_m) of the Corn-containing RNAs to assess thermal stability (Fig. 2b and Table 1). The results demonstrated that insertion of the
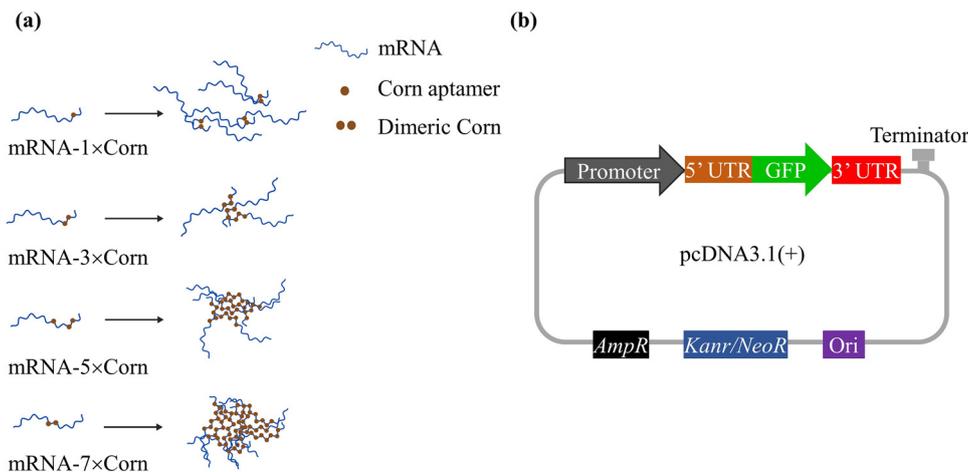
Fig. 1 Design of the UTRs for GFP mRNA and the functional elements of the plasmid constructs. (a) 3′ UTR containing different copies of the Corn RNA aptamer inserted to promote mRNA aggregation. (b) The vector pcDNA3.1(+) contains resistance genes for kanamycin (KanR) and ampicillin (AmpR), along with the origin of replication(ori). The constructs are composed of the promoter, the 5′ UTR region, the RBS, the reporter gene (GFP), a variable 3′ UTR region, and the transcriptional terminator.
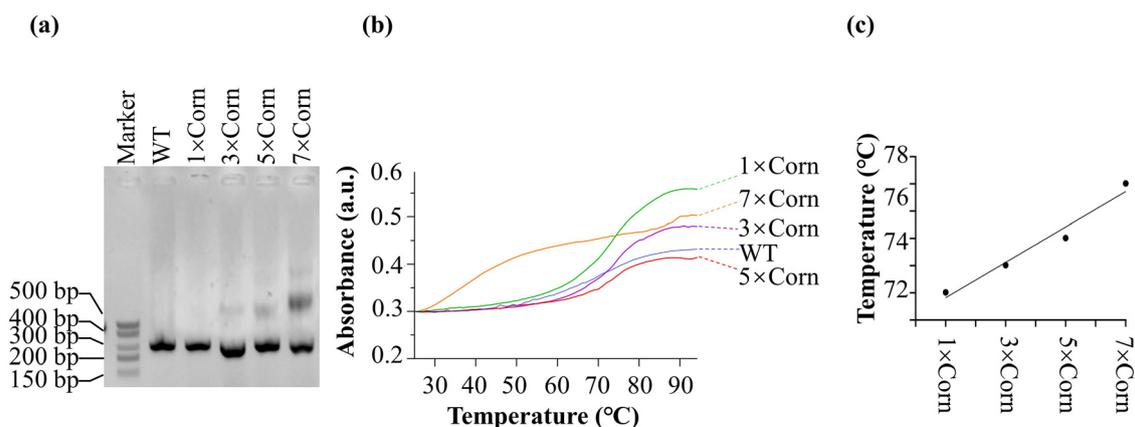

Fig. 2 The effect of Corn RNA aptamer on the formation of RNA aggregates. (a) The *in vitro* transcribed multimeric Corn RNAs analyzed by agarose gel electrophoresis. (b) The ultraviolet absorbance values at 260 nm for multimeric Corn RNAs recorded at varying temperatures. (c) Correlation analysis between the number of Corn RNA aptamer repeats and the T_m values.

Corn RNA aptamer increased the T_m value compared to the WT group. Furthermore, the T_m gradually increased with a higher number of Corn RNA aptamer repeats. The T_m of the 7 × Corn RNA increased by 8 °C compared to the WT group, indicating a significant enhancement in RNA thermal stability. Linear correlation analysis between the T_m values and the number of Corn RNA aptamer repeats yielded the fitting equation $Y = 0.65X + 72.17$, with a correlation coefficient of $R^2 = 0.9657$ (Fig. 2c).

Table 1 The T_m values of the Corn containing RNAs

Group	T_m (°C)
WT	69.0
1 × Corn	73.1
3 × Corn	74.0
5 × Corn	75.0
7 × Corn	77.0

This indicates a strong positive correlation between the number of Corn repeats and T_m, suggesting a direct relationship between structural stability and the number of repeating units.

Interestingly, the denaturation curve of the 7 × Corn group exhibited a biphasic sigmoidal shape rather than a typical single sigmoidal transition. This likely arised because the extended sequence length of the 7 × Corn RNA enables the formation of new, relatively independent structural domains within the molecule. Weak interactions between these domains may lead to the lower-temperature transition peak, corresponding to the unfolding of non-*G*-quadruplex structural elements. This biphasic profile reflected the inherent structural complexity of the 7 × Corn RNA molecule.

Regulation of GFP expression by the Corn RNA aptamer

Based on our previous observation that insertion of the Corn RNA aptamer into RNA induced RNA aggregation *in vitro*, we

next transfected the recombinant plasmids into HEK 293T cells to investigate the regulatory effect of Corn on protein expression in eukaryotic cells. We first qualitatively assessed GFP protein expression 72 h after post-transfection. Compared with the GFP-WT group, the GFP-1 × Corn, GFP-3 × Corn, GFP-5 × Corn, and GFP-7 × Corn groups exhibited progressively diminished GFP fluorescence with increasing Corn repeats. And the results revealed a clear inverse correlation between the number of inserted Corn RNA aptamer repeats and GFP fluorescence

intensity. This indicated that RNA aggregates formed through multivalent Corn RNA aptamers impaired GFP expression in HEK 293T cells.

To further assess differences in GFP protein expression among the groups in HEK 293T cells, we employed flow cytometry and western blotting to quantitatively measure GFP levels (Fig. 3a and b). Consistent with the qualitative fluorescence observations shown in Fig. S4, quantitative analysis revealed a progressive decrease in GFP fluorescence intensity,
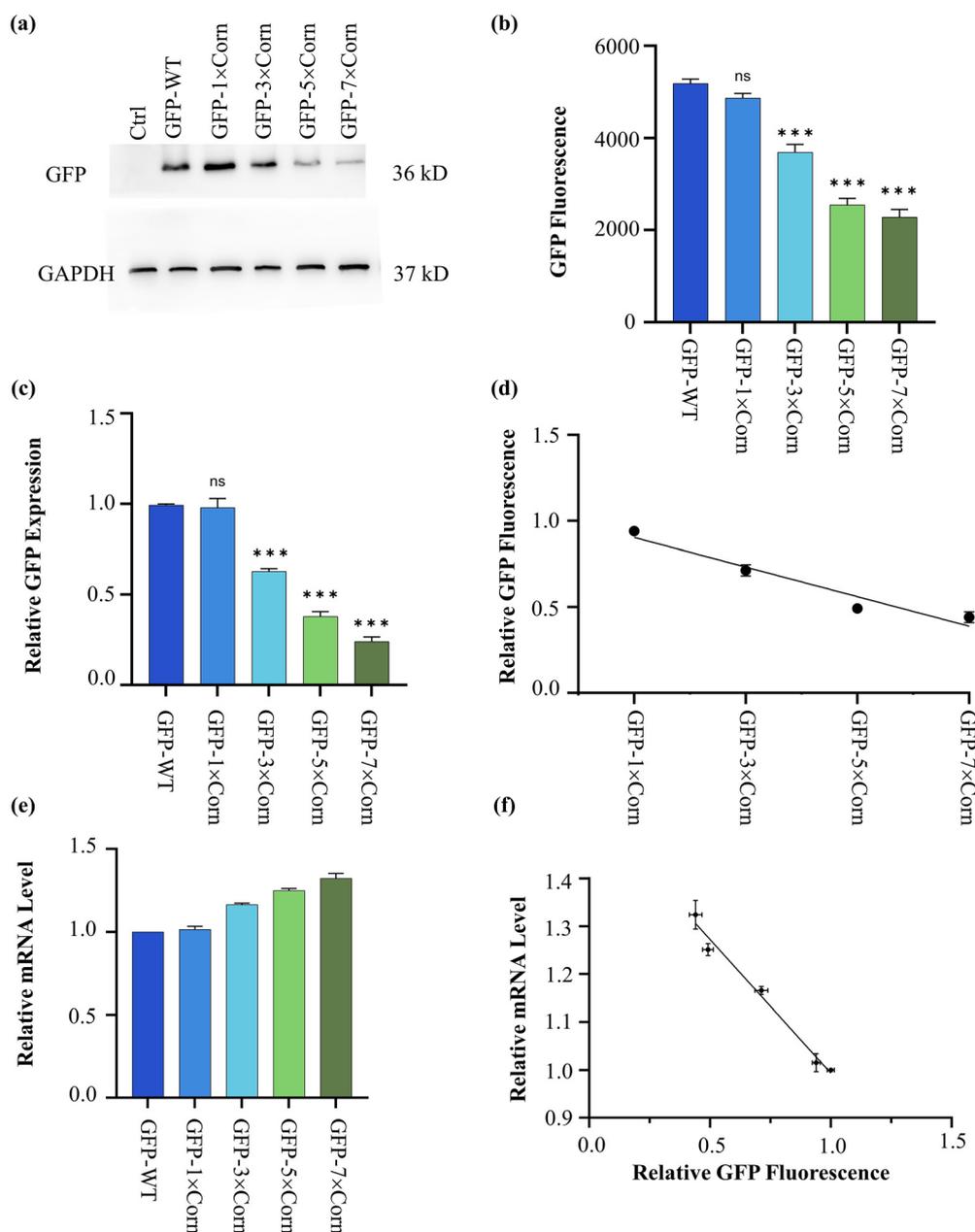

Fig. 3 Regulation of GFP expression and mRNA level by the Corn RNA aptamer. (a) Results of western blot. (b) Quantitative analysis of the expression differences of GFP in HEK 293T cells by flow cytometry. (c) Relative values of GFP expression levels in each group. (d) Correlation analysis between the relative fluorescence intensity and the number of repeats of the Corn RNA aptamer. (e) The relative content of mRNA detected by RT-qPCR. (f) Correlation analysis between mRNA stability and protein expression level. The results are presented as mean ± standard deviation (n = 3), ***p < 0.001 compared with the GFP-WT group.

as measured by flow cytometry, and a corresponding reduction in western blot band intensity across the GFP-1 × Corn, GFP-3 × Corn, GFP-5 × Corn, and GFP-7 × Corn groups compared to the GFP-WT control (Fig. 3c). This decrease correlated with an increasing number of inserted Corn RNA aptamer repeats. Linear correlation analysis between the relative fluorescence intensity and the number of Corn RNA aptamer repeats yielded the equation $Y = -0.08592X + 0.9901$, with a correlation coefficient $R^2 = 0.9292$ (Fig. 3d). Statistical analysis of the flow cytometry results confirmed that the GFP suppression rate increased positively with the number of Corn repeats. When the number of Corn repeats reached seven, the suppression efficiency approached its maximum value, approximately 50%. Notably, no significant difference in suppression rate was observed between the GFP-5 × Corn and GFP-7 × Corn groups. These results demonstrated that RNA aggregates formed through multivalent Corn RNA aptamers impaired GFP expression in HEK 293T cells.

Regulation of mRNA levels by the Corn RNA aptamer

To elucidate the regulatory mechanism of gene expression, we examined mRNA stability and protein translation efficiency. We assessed the *in vivo* levels of GFP mRNA using reverse transcription quantitative polymerase chain reaction (RT-qPCR) (Fig. 3e). The RT-qPCR results revealed a progressive increase in the relative abundance of GFP mRNA with a higher number of inserted Corn RNA aptamer repeats. This observation, combined with our previous finding of elevated RNA melting temperature (T_m) measured by UV spectrophotometry, indicated that the Corn RNA aptamer enhanced the stability of GFP mRNA within the cells. Furthermore, we performed linear correlation analysis between the relative mRNA abundance in the GFP-WT, GFP-1 × Corn, GFP-3 × Corn, GFP-5 × Corn, and GFP-7 × Corn groups and the previously measured relative GFP protein fluorescence intensity from flow cytometry. The analysis yielded the linear fitting equation $Y = -0.5581X + 1.551$, with a correlation coefficient $R^2 = 0.9719$ (Fig. 3f). This demonstrates a strong inverse correlation between mRNA levels and protein expression. These results indicated that the Corn structures within the 3′ UTR primarily reduced protein expression by inhibiting the protein translation process.

Morphological observation of Corn RNA aptamer within cells

To further elucidate the mechanism by which the Corn RNA aptamer influences gene expression, we conducted a series of analyses. After transfecting the recombinant plasmids into cells for 48 h, we stained the cells with 3,5-difluoro-4-hydroxybenzyl-idene-imidazolinone-2-oxyme (DFHO), a dye that binds to the Corn RNA aptamer, and observed the intracellular morphology of GFP mRNA containing the Corn sequence using confocal laser scanning microscopy (CLSM).

Owing to partial spectral overlap between the green fluorescence of GFP and the yellow fluorescence generated by DFHO bound to the Corn RNA aptamer, the yellow signal is masked by the stronger green fluorescence; nevertheless, a few bright spots are still discernible in the images. Distinct nuclear bright foci were observed in cells expressing GFP fused with 1×, 3×, 5×, or 7× Corn aptamer repeats, whereas such features were absent in the GFP-WT control group (Fig. 4). We suspected that this may have resulted from GFP mRNA aggregation within the nucleus induced by the Corn aptamer. Notably, the number of these spots increased with a higher number of Corn aptamer repeats. This finding confirmed our previous hypothesis that multivalent Corn aptamers may hinder the transport of GFP mRNA through nuclear pore complexes into the cytoplasm, consequently impairing GFP protein translation.

Regulation of other genes by the Corn RNA aptamer

The regulatory effect of the Corn RNA aptamer on gene expression observed in HEK 293T cells was consistent with that in HeLa cells, where the introduction of Corn into the 3′ UTR led to reduced GFP expression (Fig. S5 and S6).

To further explore the regulatory potential of the engineered Corn RNA aptamer in other genes, we inserted multivalent Corn repeats into the 3′ UTR of a luciferase reporter gene (Fig. 5a and Fig. S7). Both flow cytometry and western blotting results demonstrated that Corn reduced luciferase expression (Fig. 5b and Fig. S8).
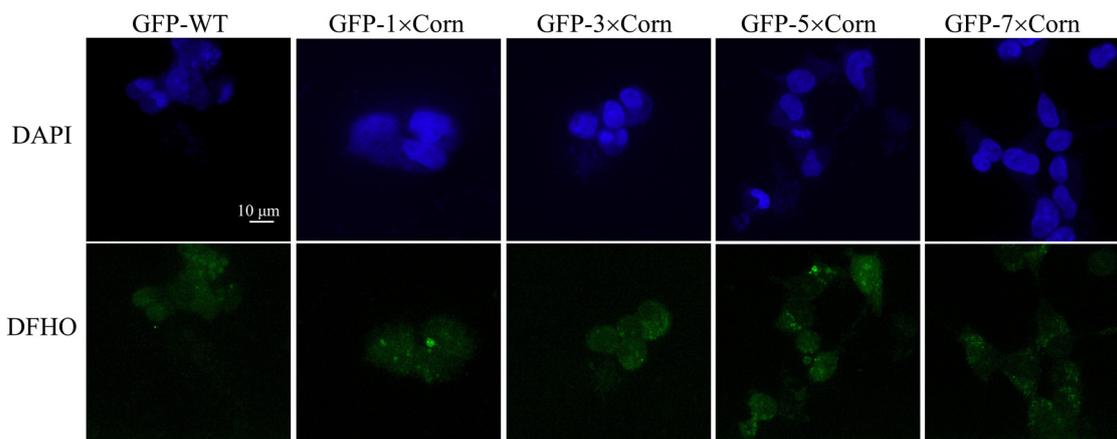

Fig. 4   The morphology of mRNA containing Corn within cells observed by confocal laser scanning microscopy. Scale bar: 10 μm.
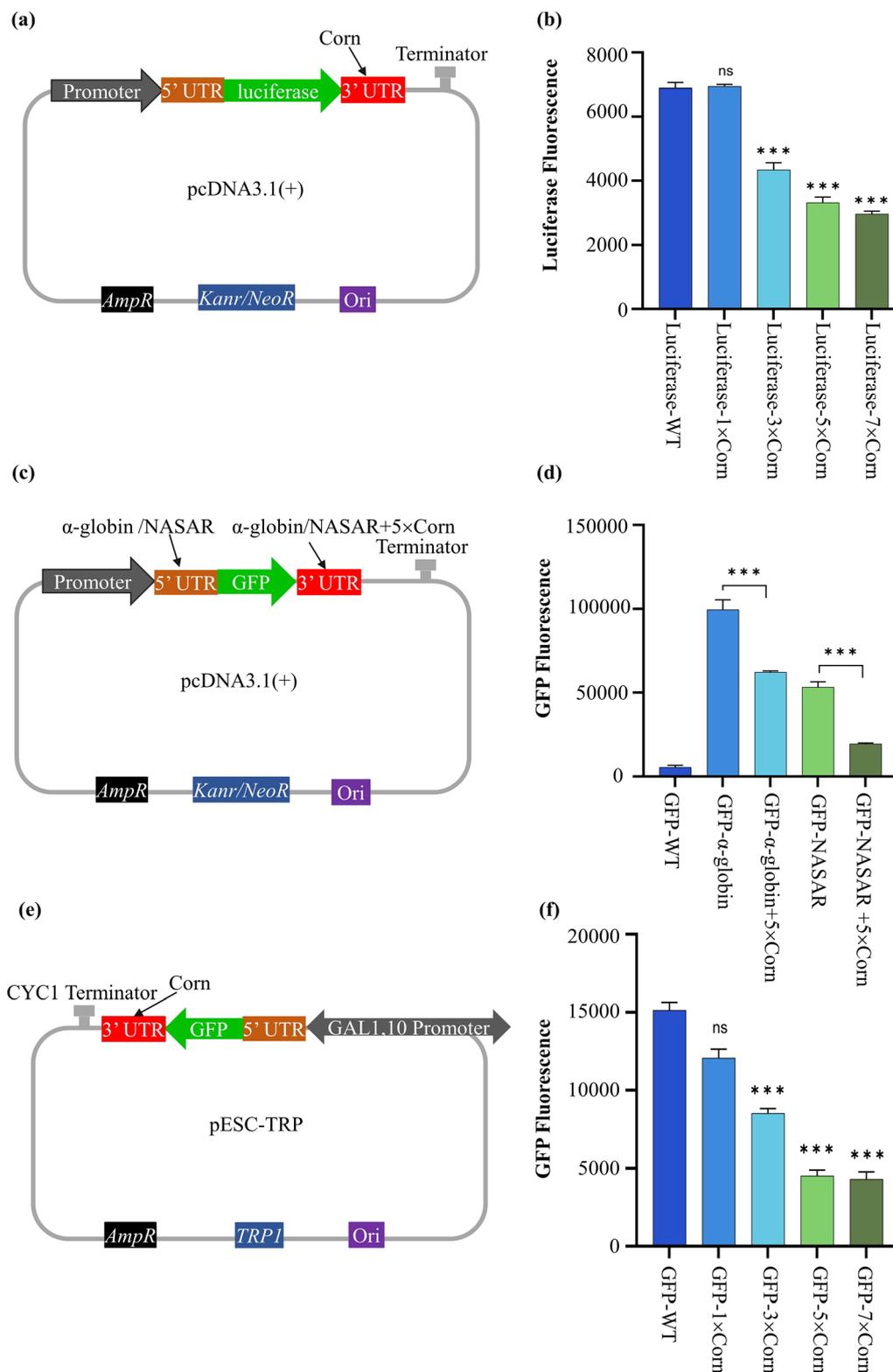
Fig. 5 Regulation of other protein expression by our designed UTRs. (a) The designed UTRs were cloned downstream of the luciferase gene to control its expression. (b) The impact of the designed UTRs on luciferase protein levels. (c) Insertion of the 5′ UTR of α-globin and NASAR upstream of GFP, and the 3′ UTR of α-globin and NASAR downstream of GFP, followed by a 5 × Corn sequence to control GFP expression. (d) The combined impact of the engineered 5′ UTR (α-globin/NASAR) and 3′ UTR (α-globin/NASAR + 5 × Corn) on GFP protein expression compared without 5 × Corn. (e) The designed UTRs were cloned downstream of the GFP gene in pESC-TRP to control its expression. (f) Quantitative analysis of the expression differences of GFP in WAT11 by flow cytometry. The results are presented as mean ± standard deviation ($n = 3$), ***$p < 0.001$ compared with the WT group.

Subsequently, we selected the human-derived α-globin gene and the NASAR UTR sequence independently designed by Dong et al.[52] (Table S1), inserting a 5 × Corn element into the 3′ UTR of both constructs (Fig. 5c). Results showed that 5 × Corn still reduced GFP protein expression (Fig. 5d), this indicated that the gene expression impairment function of our engineered Corn regulatory element is not affected by the presence of other UTR regulatory elements.

Finally, we investigated the regulatory effect of Corn in different eukaryotic expression systems. We engineered multivalent Corn RNA aptamers into the pESC-TRP expression vector within the *Saccharomyces cerevisiae* WAT11 strain (Fig. 5e and Fig. S9). Results demonstrated that Corn exerts an analogous suppressive effect on gene expression in the yeast expression system (Fig. 5f and Fig. S10, S11).

Our study establishes a novel approach for gene expression suppression. However, potential challenges and limitations remain for its application. A key consideration is whether the introduced exogenous Corn sequences impact host cell fitness. Cytotoxicity assays revealed that the insertion of the Corn RNA aptamer does not adversely affect cellular viability, proliferation, or normal cellular activities, as evidenced by healthy cell growth (Fig. S12–S14). This indicates that our method holds substantial potential for future applications.

Conclusion

In this study, we systematically investigated the regulatory function of the engineered RNA aptamer, Corn, within mRNA UTRs and its potential for gene expression control. By constructing recombinant plasmids with varying numbers of Corn repeat units, we elucidate the molecular mechanism by which this aptamer regulates gene expression through the formation of stable aggregates.

Our results demonstrated that inserting the Corn RNA aptamer into the 3′ UTR of a GFP reporter gene in eukaryotic cell models led to a significant negative correlation between the number of Corn repeats and protein expression levels. Maximum suppression efficiency (∼50%) was achieved with 7 repeats. This regulatory effect exhibits broad applicability across diverse models, including HEK 293T cells, HeLa cells, and the *Saccharomyces cerevisiae* WAT11 strain. Thermal stability analysis of *in vitro* transcribed RNA revealed that the Corn-induced G-quadruplex structures exhibited significant temperature dependence. T_m value increased progressively with the number of repeats, with the 7 × Corn RNA showing a substantial ΔT_m of +8 °C compared to wild-type, confirming a direct relationship between structural stability and repeat unit number. Native gel electrophoresis showed a pronounced reduction in RNA migration rate with increasing Corn repeats, with evident slower mobility observed for high-repeat constructs. Combined with fluorescence results observed by confocal microscopy, this steric hindrance likely impedes the interaction of mRNA with nuclear pore complexes, thus establishing that impaired nucleocytoplasmic transport

efficiency constitutes a key mechanism for the observed gene suppression.

Notably, while the Corn RNA aptamer significantly suppressed protein translation efficiency, RT-qPCR analysis revealed a concomitant increase in mRNA stability. The relative abundance of 7 × Corn RNA was approximately 1.3-fold higher compared to WT RNA. This coexistence of enhanced stability and translational suppression uncovers a dual regulatory mechanism mediated by RNA secondary structure in post-transcriptional control. Furthermore, the inhibitory effect of the Corn on GFP expression was robustly corroborated by integrated analysis using western blotting and flow cytometry. Validation of this regulatory strategy through genetic circuit experiments, where the target gene was replaced with luciferase, confirmed its broad applicability. This establishes a novel paradigm for synthetic biology component design. Critically, in terms of biosafety assessment, cytotoxicity assays and analysis of reference gene expression levels demonstrated that the introduction of the Corn did not significantly impact cellular proliferation, indicating excellent biocompatibility. This lays a crucial foundation for its potential applications in gene therapy and related fields.

In addition, the modularity and programmability of this RNA aptamer-based gene regulation system make it readily compatible with existing gene editing technologies such as the CRISPR-Cas system. By incorporating the engineered UTR elements alongside CRISPR-mediated genome modulation, synergistic control over both transcriptional and post-transcriptional processes could be achieved. This integration could enable precise spatial and temporal regulation of gene expression, allowing for fine-tuning of dosage-sensitive or context-dependent genes. For example, a CRISPR/dCas-based transcriptional activator or repressor could modulate gene transcription, while the Corn-containing 3′ UTR simultaneously governs translation efficiency and mRNA stability. Such a dual-layer regulatory strategy would substantially enhance control accuracy in cell and gene therapies.

Liu et al.[53] inserted the Corn RNA aptamer into the 3′UTR of mRNA transcribed in an *Escherichia coli* (*E. coli*) expression system, resulting in a significant increase in protein expression levels. The regulatory effects of Corn RNA aptamers on protein expression in *E. coli* and eukaryotic cells are completely opposite. We speculate that this difference may be attributed to the lack of cellular structures, such as a nucleus, in *E. coli*, a prokaryote. In *E. coli*, transcribed mRNA can form aggregates and directly interact with ribosomes in the cytoplasm for translation, without the need for nuclear export. Moreover, transcription and translation occur in coupling in *E. coli*. Since the Corn RNA aptamer is in the 3′UTR of mRNA, when the mRNA is completely transcribed and formed aggregates, each mRNA strand already carries a certain number of ribosomes. This makes it easier for ribosomes to quickly bind to the next mRNA strand after translation is completed. This thereby increased the expression level of the protein. Eukaryotic cells have more complex cellular structures and translation mechanisms. mRNA aggregates may have difficulty being transported from the nucleus to the cytoplasm and bind to ribosomes to

initiate the translation process, thus achieving the effect of gene silencing.

Our study proposed a dual post-transcriptional suppression strategy within the nucleus, in which biocompatible short-stranded RNAs self-assemble into nanostructures and induce mRNA aggregation inside the nucleus. Compared to existing technologies, this system offers distinct advantages, including enhanced design simplicity and improved biosafety. Its straightforward sequence design and reduced risk profile make it a safer alternative to gene-editing tools such as CRISPR. This study offers novel insights into the development of RNA structure–based gene regulation tools, expanding the potential applications of nucleic acid therapeutics in biomedical fields.

Conflicts of interest

The authors declare no conflict of interest.

Data availability

The data supporting this article have been included as part of the supplementary information (SI). Supplementary information: all UTR sequence and additional experimental data (agarose gel electrophoresis, cell imaging, WB, *etc.*). See DOI: **https://doi.org/10.1039/d5nh00510h**.

Acknowledgements

References

1 A. H. El-Sappah, K. Yan, Q. Huang, M. M. Islam, Q. Li, Y. Wang, M. S. Khan, X. Zhao, R. R. Mir, J. Li, K. A. El-Tarabily and M. Abbas, Comprehensive mechanism of gene silencing and its role in plant growth and development, *Front. Plant Sci.*, 2021, **12**, 705249.

2 P. Cattaneo, M. G. B. Hayes, N. Baumgarten, D. Hecker, S. Peruzzo, G. S. Aslan, P. Kunderfranco, V. Larcher, L. Zhang, R. Contu, G. Fonseca, S. Spinozzi, J. Chen, G. Condorelli, S. Dimmeler, M. H. Schulz, S. Heinz, N. Guimarães-Camboa and S. M. Evans, DOT1L regulates chamber-specific transcriptional networks during cardiogenesis and mediates postnatal cell cycle withdrawal, *Nat. Commun.*, 2022, **13**(1), 7444.

3 J. Li, T. Su, C. Zou, W. Luo, G. Shi, L. Chen, C. Fang and C. Li, Long non-coding RNA H19 regulates porcine satellite cell differentiation through miR-140-5p/SOX4 and DBN1, *Front Cell Dev. Biol.*, 2020, **8**, 518724.

4 S. Yeom, J. Oh, D. Kim and J. S. Lee, The 80(th) threonine residue of histone H3 is important for maintaining HM silencing in saccharomyces cerevisiae, *J. Microbiol. Biotechnol.*, 2024, **34**(1), 39–46.

5 R. Petroll, R. K. Papareddy, R. Krela, A. Laigle, Q. Rivière, K. Bišova, I. Mozgová and M. Borg, The expansion and diversification of epigenetic regulatory networks underpins major transitions in the evolution of land plants, *Mol. Biol. Evol.*, 2025, **42**(4), masf064.

6 E. Parperides, K. El Mounadi and H. Garcia-Ruiz, Induction and suppression of gene silencing in plants by nonviral microbes, *Mol. Plant. Pathol.*, 2023, **24**(10), 1347–1356.

7 J. Y. Cao, Y. P. Xu, W. Li, S. S. Li, H. Rahman and X. Z. Cai, Genome-wide identification of dicer-like, argonaute, and RNA-dependent RNA polymerase gene families in brassica species and functional analyses of their arabidopsis homologs in resistance to sclerotinia sclerotiorum, *Front. Plant Sci.*, 2016, **7**, 1614.

8 N. Kumar, M. Galli, J. Ordon, J. Stuttmann, K. H. Kogel and J. Imani, Further analysis of barley MORC1 using a highly efficient RNA-guided Cas9 gene-editing system, *Plant Biotechnol. J.*, 2018, **16**(11), 1892–1903.

9 P. Zhang, Z. Li, W. Cao, J. Tang, Y. Xia, L. Peng and J. Ma, A PD-L1 antibody-conjugated PAMAM dendrimer nanosystem for simultaneously inhibiting glycolysis and promoting immune response in fighting breast cancer, *Adv. Mater.*, 2023, **35**(41), e2305215.

10 Y. Huang, Q. Kou, Y. Su, L. Lu, X. Li, H. Jiang, R. Gui, R. Huang, X. Nie and J. Li, Combination therapy based on dual-target biomimetic nano-delivery system for overcoming cisplatin resistance in hepatocellular carcinoma, *J. Nanobiotechnol.*, 2023, **21**(1), 89.

11 C. Dong, J. Xiong, J. Ni, X. Fang, J. Zhang, D. Zhu, L. Weng, Y. Zhang, C. Song and L. Wang, Intracellular miRNA-triggered surface-enhanced Raman scattering imaging and dual gene-silencing therapy of cancer cell, *Anal. Chem.*, 2022, **94**(26), 9336–9344.

12 C. Zhang, S. H. Ko, M. Su, Y. Leng, A. E. Ribbe, W. Jiang and C. Mao, Symmetry controls the face geometry of DNA polyhedra, *J. Am. Chem. Soc.*, 2009, **131**(4), 1413–1415.

13 N. R. Kallenbach, R.-I. Ma and N. C. Seeman, An immobile nucleic acid junction constructed from oligonucleotides, *Nature*, 1983, **305**(5937), 829–831.

14 J. H. Chen and N. C. Seeman, Synthesis from DNA of a molecule with the connectivity of a cube, *Nature*, 1991, **350**(6319), 631–633.

15 T. J. Fu and N. C. Seeman, DNA double-crossover molecules, *Biochemistry*, 1993, **32**(13), 3211–3220.

16 F. Liu, R. Sha and N. C. Seeman, Modifying the surface features of two-dimensional DNA crystals, *J. Am. Chem. Soc.*, 1999, **121**(5), 917–922.

17 J. Zheng, J. J. Birktoft, Y. Chen, T. Wang, R. Sha, P. E. Constantinou, S. L. Ginell, C. Mao and N. C. Seeman, From molecular to macroscopic via the rational design of a self-assembled 3D DNA crystal, *Nature*, 2009, **461**(7260), 74–77.

18 Z. Ge, H. Gu, Q. Li and C. Fan, Concept and development of framework nucleic acids, *J. Am. Chem. Soc.*, 2018, **140**(51), 17808–17819.

19 K. Xia, J. Shen, Q. Li, C. Fan and H. Gu, Near-atomic fabrication with nucleic acids, *ACS Nano*, 2020, **14**(2), 1319–1337.

20 M. Cortes Jr, X. Sun, Anusha, E. J. Batchelder-Schwab, J. Li, N. Siraj, R. Jampana, Y. Zhang, Y. Bai and C. Mao, Alpha-Fold 3 modeling of DNA nanomotifs: is it reliable?, *Nanoscale Horiz.*, 2025, **10**(7), 1428–1435.

21 J. Tang, X. Jia, Q. Li, Z. Cui, A. Liang, B. Ke, D. Yang and C. Yao, A DNA-based hydrogel for exosome separation and biomedical applications, *Proc. Natl. Acad. Sci. U. S. A.*, 2023, **120**(28), e2303822120.

22 Y. Xu, Z. Lv, C. Yao and D. Yang, Construction of rolling circle amplification-based DNA nanostructures for biomedical applications, *Biomater. Sci.*, 2022, **10**(12), 3054–3061.

23 Y. Guo, Q. Zhang, Q. Zhu, J. Gao, X. Zhu, H. Yu, Y. Li and C. Zhang, Copackaging photosensitizer and PD-L1 siRNA in a nucleic acid nanogel for synergistic cancer photoimmunotherapy, *Sci. Adv.*, 2022, **8**(16), eabn2941.

24 L. Zhang, J. Chen, M. He and X. Su, Molecular dynamics simulation-guided toehold mediated strand displacement probe for single-nucleotide variants detection, *Exploration*, 2022, **2**(1), 20210265.

25 J. Wei, C. Ji, Y. Wang, J. Tan, Q. Yuan and W. Tan, Nucleic acid probes for single-molecule localization imaging of cellular biomolecules, *Chem. Biomed. Imag.*, 2023, **1**(1), 18–29.

26 Y. Zhao, X. Zuo, Q. Li, F. Chen, Y. R. Chen, J. Deng, D. Han, C. Hao, F. Huang, Y. Huang, G. Ke, H. Kuang, F. Li, J. Li, M. Li, N. Li, Z. Lin, D. Liu, J. Liu, L. Liu, X. Liu, C. Lu, F. Luo, X. Mao, J. Sun, B. Tang, F. Wang, J. Wang, L. Wang, S. Wang, L. Wu, Z. S. Wu, F. Xia, C. Xu, Y. Yang, B. F. Yuan, Q. Yuan, C. Zhang, Z. Zhu, C. Yang, X. B. Zhang, H. Yang, W. Tan and C. Fan, Nucleic acids analysis, *Sci. China: Chem.*, 2021, **64**(2), 171–203.

27 S. Stangherlin and J. Liu, Nanomaterials enabled and enhanced DNA-based biosensors, *J. Mater. Chem. B*, 2023, **11**(30), 6994–7003.

28 C. Xue, S. Zhang, C. Li, X. Yu, C. Ouyang, Y. Lu and Z. S. Wu, Y-Shaped backbone-rigidified triangular DNA scaffold-directed stepwise movement of a DNAzyme walker for sensitive microRNA imaging within living cells, *Anal. Chem.*, 2019, **91**(24), 15678–15685.

29 J. Li, S. Khan, J. Gu, C. D. M. Filipe, T. F. Didar and Y. Li, A simple colorimetric Au-on-Au tip sensor with a new functional nucleic acid probe for food-borne pathogen salmonella typhimurium, *Angew. Chem., Int. Ed.*, 2023, **62**(20), e202300828.

30 J. Li, A. A. Green, H. Yan and C. Fan, Engineering nucleic acid structures for programmable molecular circuitry and intracellular biocomputation, *Nat. Chem.*, 2017, **9**(11), 1056–1067.

31 W. Xu, W. He, Z. Du, L. Zhu, K. Huang, Y. Lu and Y. Luo, Functional nucleic acid nanomaterials: development,

properties, and applications, *Angew. Chem., Int. Ed.*, 2021, **60**(13), 6890–6918.

32 C. Zhou, Y. Song, X. Jin, B. Li and C. Pang, Construction of a scalable DNA computing nano-system for large-scale and complex logical operations, *Nanoscale Horiz.*, 2023, **8**(2), 176–184.

33 R. Wang, X. Wang, S. Xie, Y. Zhang, D. Ji, X. Zhang, C. Cui, J. Jiang and W. Tan, Molecular elements: novel approaches for molecular building, *Philos. Trans. R. Soc., B*, 2023, **378**(1871), 20220024.

34 Y. Guo, F. Wang, S. Wan, X. Liu, Y. Huang, M. Xie, X. Wei, W. Zhu, T. Yao, Y. Li, C. Zhang and Y. Zhu, Endothelium-targeted NF-κB siRNA nanogel for magnetic resonance imaging and visualized-anti-inflammation treatment of atherosclerosis, *Biomaterials*, 2025, **314**, 122897.

35 A. Khaled, S. Guo, F. Li and P. Guo, Controllable self-assembly of nanoparticles for specific delivery of multiple therapeutic molecules to cancer cells using RNA nanotechnology, *Nano Lett.*, 2005, **5**(9), 1797–1808.

36 F. Haque, D. Shu, Y. Shu, L. S. Shlyakhtenko, P. G. Rychahou, B. M. Evers and P. Guo, Ultrastable synergistic tetravalent RNA nanoparticles for targeting to cancers, *Nano Today*, 2012, **7**(4), 245–257.

37 W. W. Grabow, P. Zakrevsky, K. A. Afonin, A. Chworos, B. A. Shapiro and L. Jaeger, Self-assembling RNA nanorings based on RNAI/II inverse kissing complexes, *Nano Lett.*, 2011, **11**(2), 878–887.

38 K. A. Afonin, M. Kireeva, W. W. Grabow, M. Kashlev, L. Jaeger and B. A. Shapiro, Co-transcriptional assembly of chemically modified RNA nanoparticles functionalized with siRNAs, *Nano Lett.*, 2012, **12**(10), 5192–5195.

39 K. A. Afonin, M. Viard, A. Y. Koyfman, A. N. Martins, W. K. Kasprzak, M. Panigaj, R. Desai, A. Santhanam, W. W. Grabow, L. Jaeger, E. Heldman, J. Reiser, W. Chiu, E. O. Freed and B. A. Shapiro, Multifunctional RNA nanoparticles, *Nano Lett.*, 2014, **14**(10), 5662–5671.

40 J. B. Lee, J. Hong, D. K. Bonner, Z. Poon and P. T. Hammond, Self-assembled RNA interference microsponges for efficient siRNA delivery, *Nat. Mater.*, 2012, **11**(4), 316–322.

41 Y. H. Roh, J. Z. Deng, E. C. Dreaden, J. H. Park, D. S. Yun, K. E. Shopsowitz and P. T. Hammond, A Multi-RNAi micro-sponge platform for simultaneous controlled delivery of multiple small interfering RNAs, *Angew. Chem., Int. Ed.*, 2016, **55**(10), 3347–3351.

42 T. Kim, H. S. Han, K. Yang, Y. M. Kim, K. Nam, K. H. Park, S. Y. Choi, H. W. Park, K. Y. Choi and Y. H. Roh, Nanoengineered polymeric RNA nanoparticles for controlled biodistribution and efficient targeted cancer therapy, *ACS Nano*, 2024, **18**(11), 7972–7988.

43 F. Yang, S. Li, R. Yuan and Y. Xiang, A bivalent aptamer and terminus-free siRNA junction nanostructure for targeted gene silencing in cancer cells, *J. Mater. Chem. B*, 2022, **10**(40), 8315–8321.

44 D. Shu, H. Li, Y. Shu, G. Xiong, W. E. Carson, F. Haque, R. Xu and P. Guo, Systemic delivery of anti-miRNA for

suppression of triple negative breast cancer utilizing RNA nanotechnology, *ACS Nano*, 2015, **9**(10), 9731–9740.

45 S. Hoeprich, Q. Zhou, S. Guo, D. Shu, G. Qi, Y. Wang and P. Guo, Bacterial virus phi29 pRNA as a hammerhead ribozyme escort to destroy hepatitis B virus, *Gene Ther.*, 2003, **10**(15), 1258–1267.

46 D. Shu, Y. Shu, F. Haque, S. Abdelmawla and P. Guo, Thermodynamically stable RNA three-way junction for constructing multifunctional nanoparticles for delivery of therapeutics, *Nat. Nanotechnol.*, 2011, **6**(10), 658–667.

47 L. Sjekloća and A. R. Ferré-D'Amaré, Binding between G quadruplexes at the homodimer interface of the Corn RNA aptamer strongly activates Thioflavin T fluorescence, *Cell Chem. Biol.*, 2019, **26**(8), 1159–68.e4.

48 H. Kwon, M. Kim, Y. Seo, Y. S. Moon, H. J. Lee, K. Lee and H. Lee, Emergence of synthetic mRNA: In vitro synthesis of mRNA and its applications in regenerative medicine, *Biomaterials*, 2018, **156**, 172–193.

49 A. Wadhwa, A. Aljabbari, A. Lokras, C. Foged and A. Thakur, Opportunities and challenges in the delivery of mRNA-based vaccines, *Pharmaceutics*, 2020, **12**(2), 102.

50 A. G. Hinnebusch, I. P. Ivanov and N. Sonenberg, Translational control by 5'-untranslated regions of eukaryotic mRNAs, *Science*, 2016, **352**(6292), 1413–1416.

51 E. Matoulkova, E. Michalova, B. Vojtesek and R. Hrstka, The role of the 3' untranslated region in post-transcriptional regulation of protein expression in mammalian cells, *RNA Biol.*, 2012, **9**(5), 563–576.

52 C. Zeng, X. Hou, J. Yan, C. Zhang, W. Li, W. Zhao, S. Du and Y. Dong, Leveraging mRNA sequences and nanoparticles to deliver SARS-CoV-2 antigens in vivo, *Adv. Mater.*, 2020, **32**(40), e2004452.

53 M. Liu, Z. Jin, Q. Xiang, H. He, Y. Huang, M. Long, J. Wu, C. Zhi Huang, C. Mao and H. Zuo, Rational design of untranslated regions to enhance gene expression, *J. Mol. Biol.*, 2024, **436**(22), 168804.